Switched Ratiometric Lock-In Amplifier Enabling sub-ppm Measurements in a Wide Frequency Range

G. Gervasoni, M. Carminati, and G. Ferrari[a)]

Dipartimento di Elettronica, Informazione e Bioingegneria, Politecnico di Milano, 20133, Milano, Italy

Lock-in amplifiers (LIAs) are extensively used to perform high-resolution measurements. Ideally, when using LIAs, it would be possible to measure a minimum signal variation limited by the instrument input equivalent noise at the operating frequency and the chosen filtering bandwidth. Instead, digital LIAs show an unforeseen 1/f noise at the instrument demodulated output, proportional to the signal amplitude that poses a fundamental limit to the minimum detectable signal variation using the lock-in technique. In particular, the typical resolution limit of fast operating LIAs (> 1 MHz) is of tens of ppm, orders of magnitude worse than the expected value. A detailed analysis shows that the additional noise is due to slow fluctuations of the signal gain from the generation stage to the acquisition one, mainly due to the digital-to-analog and analog-to-digital converters. To compensate them, a switched ratiometric technique based on two analog-to-digital converters alternately acquiring the signal coming from the device under test and the stimulus signal has been conceived. An FPGA-based LIA working up to 10 MHz and implementing the technique has been realized and results demonstrate a resolution improvement of more than an order of magnitude (from tens of ppm down to sub-ppm values) compared to standard implementations working up to similar frequencies. The technique is generally applicable without requiring calibration nor ad-hoc experimental arrangements.

I. INTRODUCTION

The lock-in technique is extensively used for synchronous (phase-sensitive) AC signals detection and measurement in a wide range of scientific fields[1], spanning from Atomic Force Microscopy (AFM)[2,3] and Raman spectroscopy[4], to sensors and actuators (e.g. MEMS)[5-8].

Compared to a DC measurement approach, where the signal of interest could be overwhelmed by the 1/f noise of the electronic analog circuits, the lock-in approach shifts the stimulus signal at frequencies where the 1/f noise is negligible (only white noise for instance), thus improving the achievable signal-to-noise ratio (SNR). Then, a homodyne demodulation down-converts the signal to baseband and a low-pass filter sets the bandwidth of the measurement, independently of the modulation frequency. Benchtop digital

[a)] Author to whom correspondence should be addressed. Electronic mail: giorgio.ferrari@polimi.it

This manuscript was accepted by Rev. Sci.Instrum. Click here to see the version of record.

lock-in amplifiers (LIAs) commonly implement a homodyne detection in the digital domain to overcome the limitations of analog multipliers in terms of dynamic range, voltage offset and output noise.

A digital demodulator is expected free from 1/f noise and by operating the digital LIA at frequencies where the noise of the analog circuitry is white, the noise level at the output of the instrument could be ideally reduced at an arbitrarily small value by narrowing the bandwidth of the low-pass filter. Instead, when trying to increase the measurement resolution by narrowing the filtering bandwidth, we have experimentally verified that at a certain point the noise stops to decrease and the LIA reaches its ultimate resolution limit. LIAs resolution, usually expressed in ppm, is here defined as the ratio between the minimum detectable signal amplitude variation and the total signal amplitude, assuming detectable a signal variation equal to the rms noise (SNR = 1). For example, when measuring a signal of 1 V, if the LIA has a resolution of 1 ppm, it can sense a signal variation as tiny as 1 μV.

Table I shows the resolution experimentally measured with different LIAs when the sinusoidal stimulus signal is directly connected to the input of the instrument. The bandwidth was set to 1 Hz and the resolution is calculated on a time duration of 100 s.

TABLE I. Experimental comparison of digital LIA performances. Test conditions are: stimulus signal directly connected to the LIA input, bandwidth of 1 Hz, measurement time of 100 s and the signal amplitude and measurement frequency reported in the table.

Model	Maximum frequency [MHz]	Signal amplitude [V]	Measurement frequency [MHz]	Relative resolution [ppm]
Custom LIA[9]	0.1	0.1, 0.3, 1	0.01, 0.05	1
SR830 Stanford Research	0.1	0.1, 0.3, 1	0.01, 0.05	12
MCL1-540 SynkTek AB	0.5	1.4	0.1	1.3
SR865 Stanford Research	2	0.3	0.5	45
Custom LIA[10]	10	0.03, 0.1, 0.3, 1	0.1, 1	9
HF2LI Zurich Instruments	50	0.03, 0.1, 0.3, 1	0.1, 1, 10	39
Enhanced-LIA [This work]	10	0.1, 0.3, 1	0.0001-6 6-10	0.6-1 1-3.5

This manuscript was accepted by Rev. Sci.Instrum. Click here to see the version of record.

Results show that the instruments resolution limit cannot be improved by increasing the stimulus amplitude or by changing the operating frequency. Moreover, it was verified that also narrowing the filtering bandwidth (BW < 1 Hz) was not effective. The LIAs resolution turns out to be related to the instrument maximum operating frequency, from few ppm (for LIAs operating up to few hundreds of kHz), to few tens of ppm for instruments operating up to few MHz or tens of MHz. The distinctive results obtained with the novel Enhanced-LIA (ELIA) here presented are reported in the last row.

To overcome the LIA resolution limit and carry out high resolution measurements, one possible approach is to perform differential measurement[11]. A simple example of differential scheme for the measurement of the impedance Z_{DUT} of a device under test (DUT) is the well-known Wheatstone bridge reported in Fig. 1. The instrument measures the difference A_{DIFF} between the DUT signal A_{DUT} and a reference signal A_{REF}, both generated starting from the same stimulus voltage V_{OUT}. The resolution limit of the LIA is proportional to the A_{DIFF} signal, which in case of a well-balanced bridge is a value near to null. As consequence, the resolution limit of the LIA is negligible and it is practically possible to measure very small variations of Z_{DUT}. When using this approach, the more the reference signal is similar (at any given time) to the DUT signal, the smaller is the differential signal and the less the resolution limit of the LIA counts. This widely used technique allows measurement with resolution lower than 1 ppm, as reported for capacitance bridges[12,13].

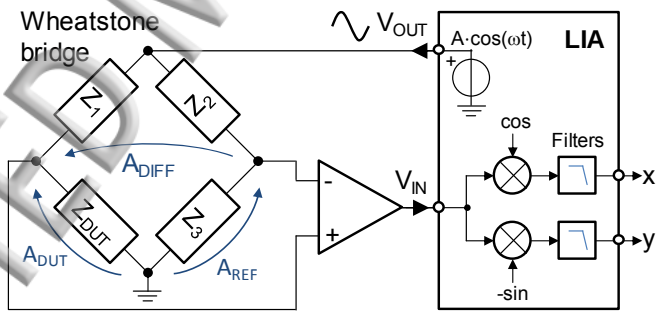

FIG. 1. Example of differential configuration (Wheatstone bridge) for high-resolution measurements of the sample impedance Z_{DUT} by means of a lock-in amplifier (LIA).

Although the differential approach allows obtaining excellent results, the generation of a well-balanced reference signal could be cumbersome. The amplitude and phase of the reference signal should match the DUT signal for every bias condition, operating temperature and frequency of measurement. Consequently, a calibration process is generally required for every DUT and measurement condition, adding complexity to the system and to the measurement itself.

In this work, we present a technique for the reduction of the low-frequency noise at the demodulated output of a digital LIA. It allows the design of a general-purpose digital LIA with sub-ppm resolution, not requiring calibration steps, nor additional elements to the setup or limitations on the DUT parameters. The paper is organized as follows. Section II discusses the sources of noise that limit the resolution of a digital LIA. The technique for the noise reduction is described in section III. The experimental validation of the system is reported in section IV. Finally, section V summarizes the main results and concludes the paper.

II. RESOLUTION LIMIT OF DIGITAL LIAs

A. Experimental Assessment of the Resolution Limits

To understand the results reported in Table I, the noise of the state-of-the-art lock-in amplifier HF2LI by Zurich Instruments has been characterized and analyzed in depth. A 1 MHz sinusoidal stimulus ranging from 0 to 1 V has been generated at the instrument output and directly connected to its input (Fig. 2, top). In all measurements, the input and output ranges have been set at 1.1 V and 1 V respectively. The signal, after synchronous demodulation, is filtered (80 kHz bandwidth) and acquired. The FFT is performed and the results are shown in Fig 2.

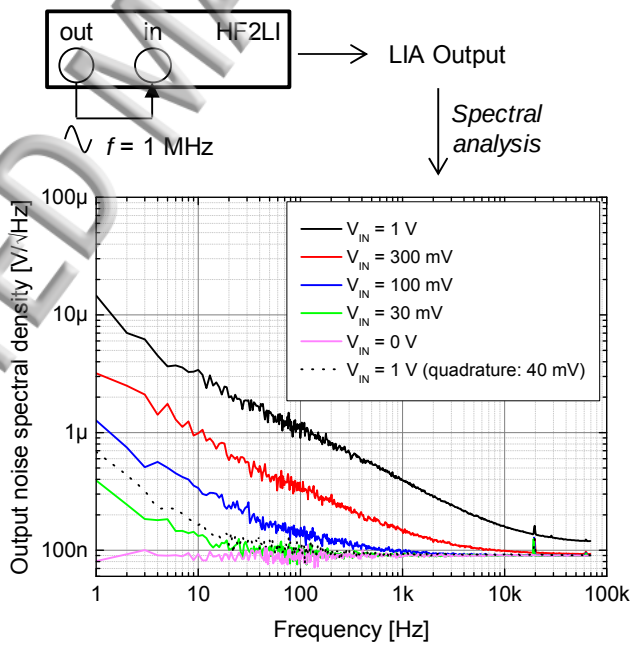

FIG. 2. Noise spectral densities of the demodulated LIA output obtained directly connecting the output terminal to the input of the commercial HF2LI. In addition to the white noise, a 1/f contribution proportional to the signal amplitude is present. The dashed line refers to the noise in the quadrature output with an in-phase component of 1 V and a quadrature component of 40 mV.

In the absence of a forcing signal (stimulus voltage V_{OUT} set to 0 V) the demodulated signal shows a white noise equal to the noise of the analog front-end at 1 MHz, as expected. However, as the sinusoidal signal amplitude increases, additional 1/f noise proportional to the signal amplitude appears. The same behavior has been observed with all tested LIAs.

This signal-proportional 1/f noise produces two drawbacks: i) due to the 1/f spectral distribution, narrowing the filter bandwidth is no more effective in order to reduce the output noise of the instrument; ii) increasing the signal amplitude does not improve the measurement resolution due to the noise concomitant increase. As a consequence, when dominated by this 1/f noise, the LIA reaches its ultimate resolution limit.

This limitation is confirmed by Fig. 3, which shows the resolution obtained using the same setup of Fig. 2 and varying the signal amplitude (from 0 to 1 V). For comparison, the figure also reports the expected theoretical results considering only the instrument white noise measured for V_{OUT} = 0 V. By increasing the signal amplitude, the resolution reaches a plateau of about 40 ppm independently of the measuring bandwidth fixed by the low-pass filter. The resolution degradation due to the additional 1/f noise turns out to be remarkable. For example, with a 1 V signal amplitude and 10 Hz low-pass filter, it would be ideally achievable a noise of 280 nV_{rms} and a corresponding resolution of about 0.28 ppm. Instead, the measured resolution turns out to be only 40 ppm, a factor 140 worse.

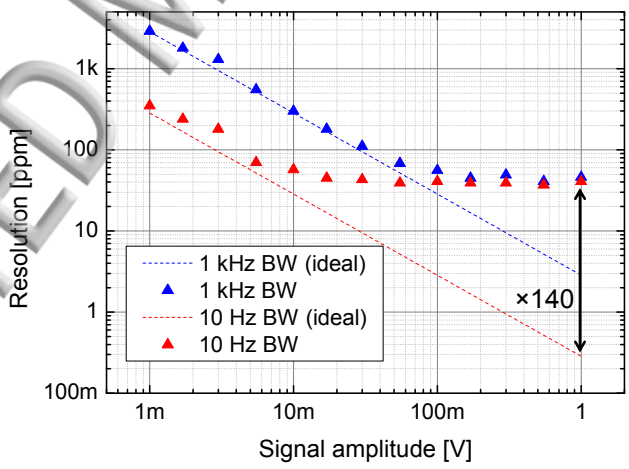

FIG. 3. Resolution obtained with the HF2LI (directly connecting output and input of the instrument as shown in Fig. 2 and performing measurements 100 s long) for different signal amplitudes and two filtering bandwidths (1 kHz and 10 Hz). The dashed lines are the theoretical resolution of the instrument by considering only the noise of the input analog stages.

B. Identification of Flicker Noise Sources

As already mentioned in Sec. I, benchtop digital LIAs implement homodyne detection in the digital domain, which is ideally free from 1/f noise. Since the additional 1/f noise is proportional to the signal

amplitude, the role of the waveform generator of the LIA has been investigated. The noise added to the sinusoidal waveform by the output stage of the generator is modulated by the digital demodulator of the LIA giving a non-flicker noise at the output of the instrument, thus cannot explain our results. The phase noise of the generator has been discarded as well. In fact, although its contribution is proportional to the signal, it would produce a noise level of the quadrature term higher than the noise of the in-phase term (Ref. 1, pp. 71-73). On the contrary, experimental evidence (Fig. 2, dashed line) shows a noise of the quadrature component much smaller than the in-phase noise.

A further noise term of a waveform generator is the amplitude noise. A random modulation of the amplitude of the sinusoidal signal is down-converted by the LIA giving an additional noise in the in-phase component (or in the signal amplitude modulus), in agreement with the experimental results. Indeed, every component defining the amplitude of the signal, not only in the generation chain, but also in the acquisition one, is a source of a signal amplitude modulation if its gain fluctuates.

For example, the unavoidable 1/f noise of the analog reference voltage used by the digital-to-analog converter (DAC) and the analog-to-digital converter (ADC) results in signal amplitude modulation. In fact, if the DAC reference voltage increases, the corresponding output voltage range is stretched and signal amplitude increases, while if the ADC reference voltage increase, the digital signal processed by the LIA decreases. Similar effects can be originated from internal circuits of the DAC and ADC that define the conversion gain. Regarding the analog stages, the resistors setting the gain of the amplifiers are examples of amplitude modulation sources. The intrinsic 1/f noise and temperature fluctuations change the value of the resistors and therefore the gain experienced by the signal. Figure 4 shows the effect of these gain fluctuations in a simplified LIA schematic, where G_{DAC}, G_G and G_{ADC} are the nominal gains of DAC, input amplifier and ADC, respectively. The n_{DAC}, n_{ADC} and n_G terms summarize the converters and analog stages different contributions to the gain fluctuations. The digital processor operates the demodulation of the digital signal V_{dig} given by:

$$V_{dig}(k) = A(1 + n_{DAC})|T_{DUT}|G_G(1 + n_G)(1 + n_{ADC})\sin(2\pi f_0 k T_s + \phi_{DUT}) \quad (1)$$

where A is the amplitude of the stimulus voltage, $|T_{DUT}|$, ϕ_{DUT} are the magnitude and phase at f_0 of the DUT transfer function, T_s is the sampling period and k is an integer. The amplitude R measured by the LIA is

This manuscript was accepted by Rev. Sci.Instrum. Click here to see the version of record.

$$R = A|T_{DUT}|G_G(1+n_{DAC})(1+n_G)(1+n_{ADC}) \quad (2)$$

Thus, the slow gain fluctuations n_{DAC}, n_G, n_{ADC} are reflected in slow fluctuations of the amplitude calculated by the LIA, setting the resolution limit of the instrument independently of f_0. Whatever signal is measured, it will always be affected by the LIA gain fluctuation, so if these fluctuations are in the order of tens of tens ppm, it will not be possible to measure the signal with a better resolution.

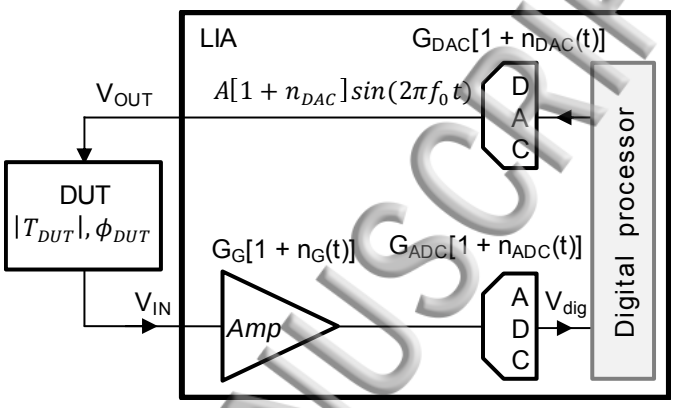

FIG. 4. Visualization of the various multiplicative blocks along the signal path in a digital LIA, affected by slow gain fluctuations which set the resolution limit as detailed in Eq. 1.

III. RATIOMETRIC LOCK-IN AMPLIFIER ARCHITECTURES

In order to enhance the LIA resolution performance, its gain fluctuations should be reduced. Regarding the analog conditioning stages, this can be obtained by using resistors with a low temperature coefficient (< 5 ppm/°C)[9] where necessary, i.e. where resistors set the signal transfer function of the instrument. Such components are less sensitive to temperature variations and are usually associated also with a low intrinsic 1/f noise (thus with lower resistance value variations). Instead, regarding the DAC and the ADC, which are the major fluctuations contributors in our custom LIAs, there are no studies suggesting a way to reduce the effect of both. The solution of a common voltage reference between the DAC and the ADC would allow the cancellation of the reference effect, but it is not effective for the internal fluctuation sources of ADC and DAC converters such as, for instance, the 1/f noise of a simple voltage buffer at the reference input.

A. Digital Switched Ratiometric LIA with a Single ADC

The effect on the measurement of the gain fluctuations added by the DAC and all the generation chain can be reduced using the ratiometric technique: the amplitude of the DUT signal is compared to the amplitude of the stimulus signal. Ratiometric techniques are a common approach for high accuracy measurements[14-16] and for the compensation of the light source intensity fluctuations in optical measurements[17]. The ratiometric technique can be easily implemented using a dual channel LIA. The acquisition of the stimulus (STIM) signal in addition to the DUT signal (Fig. 5(a)) and their separate processing with a standard lock-in approach, produces two measured amplitudes (A_{DUT} and A_{STIM}), both proportional to the gain fluctuations of the DAC (and generation stage). Thus, a division between the two amplitudes gives a value independent of the fluctuations of the generation stage. The phase can be retrieved as a simple difference between the DUT phase ϕ_{DUT} and the STIM phase ϕ_{STIM}. Since the phase is less sensitive to a random amplitude modulation, in the following we only analyze the measurement of the amplitude.

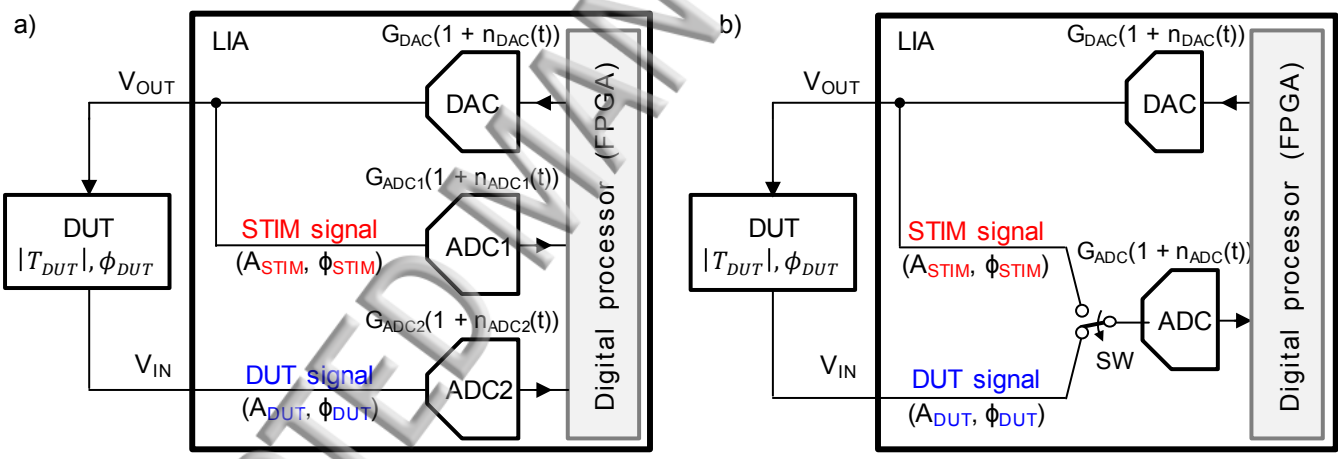

$$A_{DUT} = A|T_{DUT}| \cdot (1 + n_{DAC}(t)) \cdot (1 + n_{ADC1}(t))$$
$$A_{STIM} = A \cdot (1 + n_{DAC}(t)) \cdot (1 + n_{ADC2}(t))$$
$$A_{DUT}/A_{STIM} = |T_{DUT}| \cdot (1 + n_{ADC1}(t))/(1 + n_{ADC2}(t))$$

$$A_{DUT} = A|T_{DUT}| \cdot (1 + n_{DAC}(t)) \cdot (1 + n_{ADC}(t))$$
$$A_{STIM} = A \cdot (1 + n_{DAC}(t)) \cdot (1 + n_{ADC}(t))$$
$$A_{DUT}/A_{STIM} = |T_{DUT}|$$

FIG. 5. (a) Simplified scheme implementing a ratiometric measurement using two ADCs. (b) Simplified scheme of a switched ratiometric LIA based on a single ADC. For visual clarity, the effect of the analog stages is not considered.

This standard ratiometric approach was experimentally verified to improve the resolution of the measurement by less than a factor two. The lack of efficacy is due to the gain fluctuations of the two independent ADCs, which are not compensated. In order to remove also their effect, a switched ratiometric approach has been conceived. A first single-ADC version relies on the acquisition of both DUT and the STIM signals with the same ADC, which allows them to be equally affected by the ADC gain fluctuations

and consequently to cancel out their effect through a ratio operation. Figure 5(b) shows the architecture of this switched ratiometric LIA with single ADC. A switch SW periodically changes the input of the ADC alternating the DUT and the STIM signals. The switching frequency is chosen fast enough to assume the same ADC gain for the DUT samples and the STIM samples in a switching period. The digital processor separates the digitized samples to reconstruct the two signals in the digital domain, implements the synchronous demodulation of them and finally calculates the ratio of the amplitudes. Although the gain fluctuations are slow (up to few kHz from Fig. 2), the switching frequency of SW should be chosen fast enough to satisfy the sampling theorem in order to avoid loss of information. Such a condition is difficult to be fulfilled in the case of high frequency digital LIAs, with sampling rate of tens or hundreds of MS/s, due to the voltage transients given by the switching of the ADC input.

B. Ratiometric LIA Based on Two ADCs

To reduce the switching frequency required by the scheme of Fig. 5(b), an architecture based on two ADCs, as shown in Fig. 6, is proposed[18] and implemented. Two switches SW1 and SW2 are added in front of the ADCs to alternatively acquire the DUT and the STIM signals with each ADC. The signals are reconstructed in real-time using a FPGA to obtain their time evolution with continuity in the digital domain. The following demodulation and averaging are performed as in a standard dual-phase LIA obtaining amplitude and phase of the DUT and STIM signals. The switching frequency f_{SW} of SW1 and SW2 is chosen higher than the 1/f noise corner of the slow random gain fluctuations of the ADCs, few kHz in our prototype. Consequently, the equivalent mean gain in each period $1/f_{SW}$ experienced by the two reconstructed signals is the same and is equal to the mean of the two ADC gains. After demodulation and the low-pass filtering, the effect of the gain fluctuations is finally canceled out by performing the ratio between the amplitudes of the DUT and STIM signals. The gain fluctuations of the DAC are also included in both signals and therefore are removed as well, allowing a high-resolution measurement of the DUT signal.

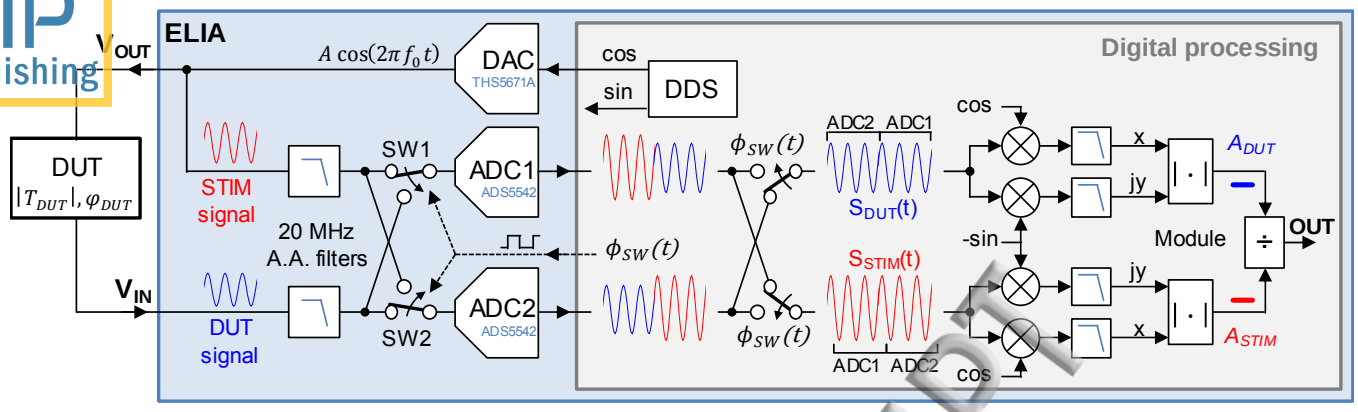

FIG. 6. Architecture of the switched ratiometric LIA scheme based on two ADCs and on digital reconstruction of the data streams.

C. Theoretical Analysis

Here the working principle of the presented switched ratiometric scheme is analyzed in detail. Then, some considerations on the harmonics generated by the switching operation and how to prevent them from causing performance degradation are made.

The ADCs alternatively acquire the stimulus signal applied to the DUT and the DUT response, as shown in Fig. 6. The two digitally reconstructed signals DUT and STIM can be represented by

$$S_{DUT}(t) = A|T_{DUT}|\cos(2\pi f_0 t + \varphi_{DUT}) \times [G_{ADC1}(t)\phi_{SW}(t) + G_{ADC2}(t)(1-\phi_{SW}(t))] \quad (3)$$

$$S_{STIM}(t) = A\cos(2\pi f_0 t) \times [G_{ADC2}(t)\phi_{SW}(t) + G_{ADC1}(t)(1-\phi_{SW}(t))] \quad (4)$$

where $\phi_{SW}(t)$ is a square wave (0 to 1) with a duty cycle of 50% and period T_{SW} as shown in Fig. 7(a). $G_{ADC1}(t)$ and $G_{ADC2}(t)$ are the gains of the two ADCs at the time t. For simplicity, it is assumed $\varphi_{DUT} = 0$ and are neglected the noise of DAC, analog stages and quantization.

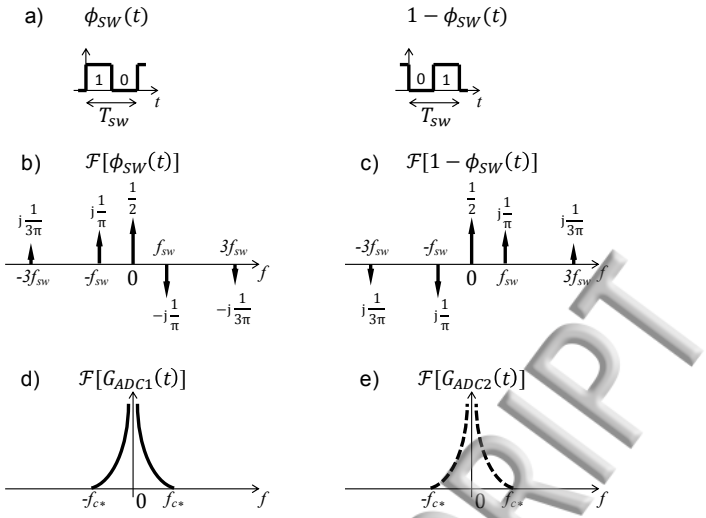

FIG. 7. Spectra of DUT and STIM signals after reconstruction in the digital domain for different f_0 and f_{SW}.

These reconstructed signals are demodulated in phase and quadrature by the lock-in amplifier. The in-phase component obtained by a multiplication with the reference signal $\cos(2\pi f_0 t)$ is:

$$S_{DUT,demod} = \frac{A}{2}|T_{DUT}|\left[G_{ADC1}(t)\phi_{SW}(t) + G_{ADC2}(t)\left(1-\phi_{SW}(t)\right)\right] + \frac{A}{2}|T_{DUT}|\left[G_{ADC1}(t)\phi_{SW}(t) + G_{ADC2}(t)\left(1-\phi_{SW}(t)\right)\right]\cos(2\pi 2 f_0 t) \quad (5)$$

$$S_{STIM,demod} = \frac{A}{2}\left[G_{ADC2}(t)\phi_{SW}(t) + G_{ADC1}(t)\left(1-\phi_{SW}(t)\right)\right] + \frac{A}{2}\left[G_{ADC2}(t)\phi_{SW}(t) + G_{ADC1}(t)\left(1-\phi_{SW}(t)\right)\right]\cos(2\pi 2 f_0 t) \quad (6)$$

These two signals can be studied performing the Fourier transform and exploiting the convolution theorem. Although Eqs. 5 and 6 are characterized by two terms, it is useful to start taking into account only the first one, while the second one, multiplied by $\cos(2\pi 2 f_0 t)$, will be treated successively:

$$\mathcal{F}\{S_{DUT,demod,I-term}(t)\} = \frac{A}{2}|T_{DUT}| \times \{\mathcal{F}[G_{ADC1}(t)] * \mathcal{F}[\phi_{SW}(t)] + \mathcal{F}[G_{ADC2}(t)] * \mathcal{F}[1-\phi_{SW}(t)]\} \quad (7)$$

This manuscript was accepted by Rev. Sci.Instrum. Click here to see the version of record.

$$\mathcal{F}\{S_{STIM,demod,I-term}(t)\} = \frac{A}{2} \times \{\mathcal{F}[G_{ADC2}(t)] * \mathcal{F}[\phi_{SW}(t)] + \mathcal{F}[G_{ADC1}(t)] * \mathcal{F}[1-\phi_{SW}(t)]\} \quad (8)$$

To compute the Fourier transform of the two signals (Eqs. 7 and 8), it is useful to compute and represent the Fourier transform of their various terms. The Fourier transform of the square wave signals $\phi_{SW}(t)$ and $1-\phi_{SW}(t)$ are described by a series of Dirac delta functions at 0, $\pm f_{SW}$, $\pm 3f_{SW}$, etc., as represented in Figures 7(b) and (c). Although the Fourier transform should be represented by the real and imaginary part separately, for simplicity in Fig. 7 the real and imaginary parts are combined in a single graph. The Fourier transform of $G_{ADC1}(t)$ and $G_{ADC2}(t)$ are sketched in Figs 7(d, e) and are characterized by a 1/f noise which becomes negligible starting from a frequency defined f_{c*}, while their white noise is neglected. In Fig. 7 the Fourier transforms of G_{ADC1} and G_{ADC2} are qualitatively sketched with their spectral power density. The analysis uses the Fourier transform which has the important feature of keeping the phase information, unlike the power spectral density.

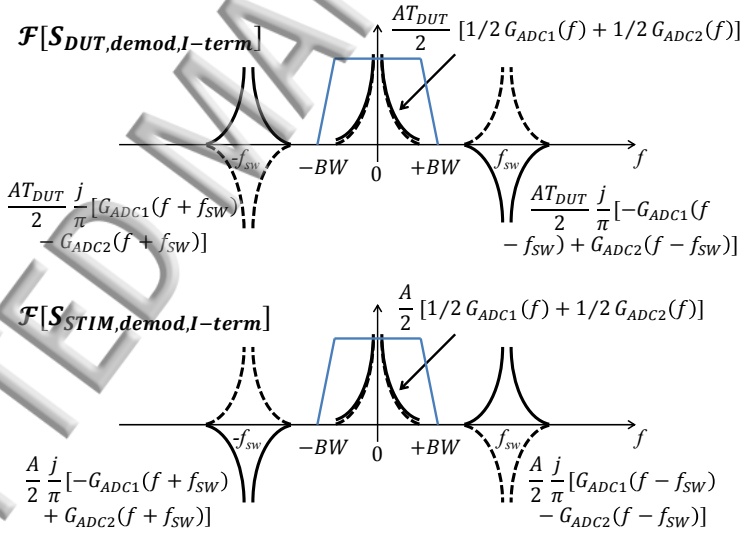

FIG. 8. Spectra obtained from the sum and convolution of the various terms of Eqs. 7 and 8. The continuous lines and the dashed lines are the components produced by G_{ADC1} and G_{ADC2}, respectively. For graphical clarity, the successive harmonics at $\pm 3f_{SW}$, $\pm 5f_{SW}$, etc. are not depicted.

In Fig. 8 the spectra obtained from the sum and convolution of the various terms are shown. In DC, both the signals of interest, $A|T_{DUT}|/2$ and $A/2$ from the demodulated signals DUT and STIM respectively, are multiplied by the same factor $[G_{ADC1}(f)+G_{ADC2}(f)]/2$. This confirm the intuitive idea that the two signals experience an equivalent mean gain given by the mean of the two ADCs gain. Instead,

the terms at $\pm f_{SW}$ and successive harmonics are multiplied by a different factor in DUT and STIM, thus the ratio of the two signals would be dependent on the converter gains. In order to make the ratio operation effective in canceling the effect of $G_{ADC1}(t)$ and $G_{ADC2}(t)$, it is necessary to filter the harmonics including their tails. This can be done by the low-pass filter already implemented in the LIA. Given a certain filtering bandwidth BW, the f_{SW} should be selected in order to make the harmonics (and tails) stay out of the bandwidth BW of the low-pass filter, that is:

$$f_{SW} > f_{c*} + BW \tag{9}$$

If this condition is satisfied, it is possible to write the signals at the output of the low-pass filters as:

$$S^{LPF}_{DUT,demod,I-term}(t) \cong \frac{A}{2}|T_{DUT}|[\frac{G^{LPF}_{ADC1}(t) + G^{LPF}_{ADC2}(t)}{2}] \tag{10}$$

$$S^{LPF}_{STIM,demod,I-term}(t) \cong \frac{A}{2}[\frac{G^{LPF}_{ADC1}(t) + G^{LPF}_{ADC2}(t)}{2}] \tag{11}$$

and performing the ratio between the two signals:

$$\frac{S^{LPF}_{DUT,demod,I-term}(t)}{S^{LPF}_{STIM,demod,I-term}(t)} \cong |T_{DUT}| \tag{12}$$

obtaining a measurement of the DUT independent of the two ADCs gain fluctuations.

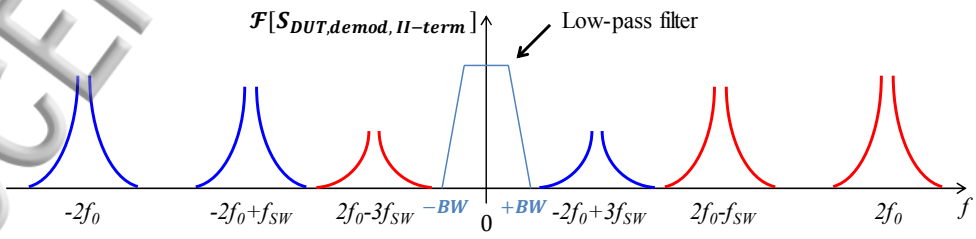

FIG. 9. Harmonics in the demodulated signal due to the term multiplied by $\cos(2\pi f_0 t)$ of Eq. 5. The harmonics must fall outside the measurement bandwidth ±BW set by the low-pass filter. The same spectral distribution is expected for the demodulated stimulus signal $S_{STIM,demod}$.

This manuscript was accepted by Rev. Sci.Instrum. Click here to see the version of record.

If the second term of Eqs. 5 and 6 is considered, others harmonics appear, in particular at the frequencies $2f_0$, $2f_0 \pm f_{SW}$, $2f_0 \pm 3f_{SW}$, …, $-2f_0$, $-2f_0 \pm f_{SW}$, $-2f_0 \pm 3f_{SW}$, ..., as shown in Fig. 9 where the modulus of the Fourier transform is represented. Also in this case it is important that the harmonics with their tails do not fall into the bandwidth of interest between ±BW. Looking at the bilateral spectrum of Fig. 9, to avoid harmonics in bandwidth ±BW it is necessary to satisfy this condition:

$$BW < 2f_0 - (1+2k)f_{SW} - f_{c*} \tag{13}$$

or this other condition:

$$2f_0 - (1+2k)f_{SW} + f_{c*} < -BW \tag{14}$$

for each natural number k. These conditions are written by considering the components produced by the $2f_0$ term (red harmonics in Fig. 9). The harmonics from $-2f_0$ (in blue) are specular and give the same conditions. In summary, the f_{SW} has to satisfy these conditions:

$$\begin{cases} f_{SW} > f_{c*} + BW \\ f_{SW} > \dfrac{2f_0 + f_{c*} + BW}{1+2k} \quad or \quad f_{SW} < \dfrac{2f_0 - f_{c*} - BW}{1+2k} \end{cases} \tag{15}$$

In addition to these conditions, it is also convenient to set a switching frequency different from f_0. The switches commutation can inject into the ADCs inputs a feedthrough signal at f_{SW} which would fall into the modulated signal bandwidth for $f_{SW} \approx f_0$.

In some practical cases, these conditions are considerably simplified. High resolution measurements commonly require a narrow bandwidth BW in order to reduce the noise of the analog stages. By assuming BW much smaller than f_{c*}, the conditions are simplified into:

$$\begin{cases} f_{SW} \gg f_{c*} \\ f_{SW} \neq f_0 \\ (1+2k)f_{SW} \neq 2f_0 \end{cases} \tag{16}$$

The last two conditions must be satisfied with a certain margin given the performed approximations.

IV. EXPERIMENTAL RESULTS

A. Enhanced-LIA realization

An Enhanced-LIA instrument (ELIA) based on the switched ratiometric technique has been implemented and fully characterized. The prototype, shown in Fig. 10, comprises a generation channel, two identical acquisition channels and is controlled by a Xilinx Spartan 6 FPGA mounted on a commercial module XEM6010 by Opal Kelly connected to the board, which also provides an USB interface to the PC running a graphical user interface for setting parameters and displaying signals. The switching of the signal at the input of the ADCs is implemented using fast CMOS single-pole double throw switches (ADG752 by Analog Devices). Random and uncorrelated fluctuations of the on resistance of the switches change the voltage divider between the switch resistance and the finite input resistance of the ADCs (about 6.6 kΩ in our case), limiting the stability of the measurement. We have chosen low resistance (15 Ω) switches to reduce these fluctuations by a factor $\approx 2 \cdot 10^{-3}$. The detailed board design is described elsewhere[19].

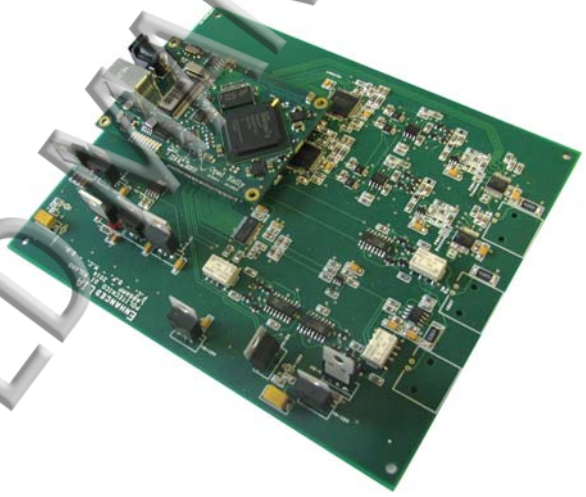

FIG. 10. Picture of the realized instrument prototype (board size 16 × 13 cm) featuring a Xilinx Spartan 6 FPGA.

In this section, the effectiveness of the switched ratiometric technique is demonstrated by showing an enhancement of the resolution limit of the LIA by more than an order of magnitude (from 9 to 0.6 ppm) without requiring a calibrated reference signal.

B. Assessment of the ELIA Resolution

This manuscript was accepted by Rev. Sci.Instrum. Click here to see the version of record.

To verify the effectiveness of the switched ratiometric technique, a sinusoidal signal of 1 V at a frequency of 1 MHz has been generated and applied to the input of ELIA through a resistive voltage divider as shown in Fig. 11(a). In the first experiment reported in Fig. 11(b), the DUT and STIM signals have been acquired with a specific ADC without switching the signals. The demodulated signals are normalized and the fluctuations appear of the same amplitude but not correlated limiting the resolution to about 9 ppm rms. Although the DAC fluctuations are shared by the two signals, the ones of the two ADCs are indeed uncorrelated, making a simple ratiometric approach ineffective. By enabling the switches to perform the proposed switched ratiometric technique, the fluctuations of the reconstructed DUT and STIM signals are clearly correlated (Fig.11(c)). Thus, they can be effectively reduced by means of a ratio operation, obtaining a residual uncertainty of 0.7 ppm in this case (Fig. 11(d)). Given the obtained results and the fact that the DUT and STIM signals are of different amplitude (0.5 and 1 V respectively), the demodulated output fluctuations cannot be related to an additive noise, but necessarily to gain fluctuations confirming the analysis in section II.

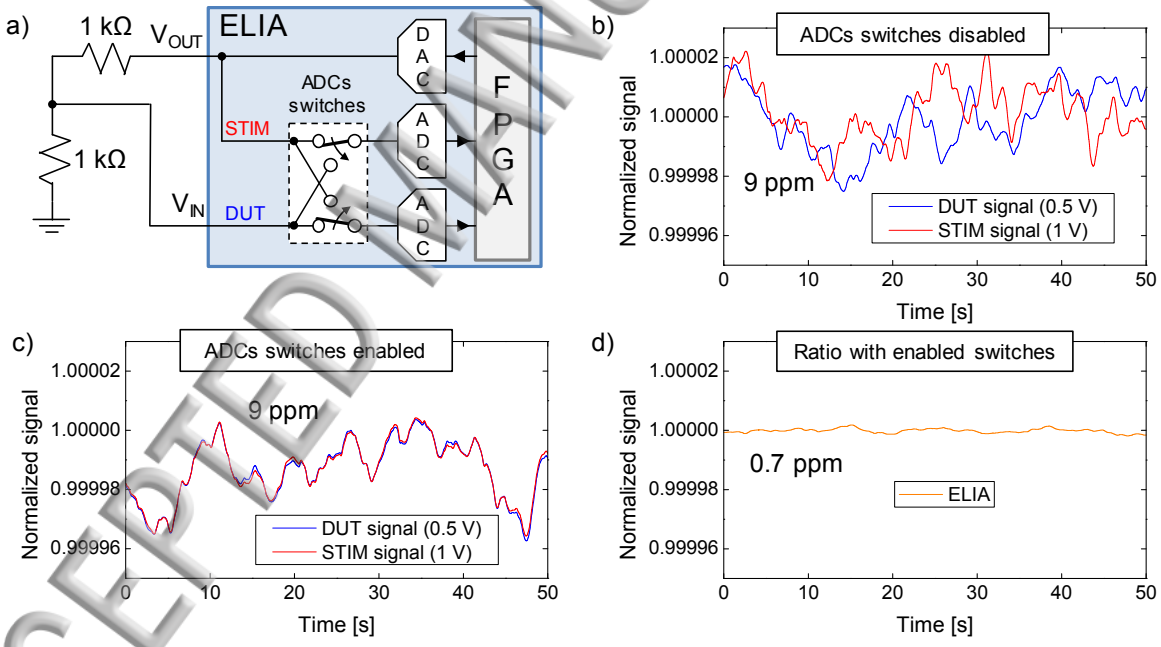

FIG. 11. Demonstration of the technique effectiveness in making the DUT and STIM signals experience the same gain fluctuations in order to allow their cancellation by means of a simple ratio: (a) test setup, processed signals when (b) the switches are disabled (standard LIA operation) and (c) the switching is enabled (enhanced mode). (d) output of the instrument (ratio).

To evaluate the ELIA performance, Fig. 12(b) shows the tracking of a time-varying resistance of 250 Ω periodically changed (period of 10 s) of ΔR = 1.25 mΩ, i.e. 5 ppm. The signal amplitude applied to the time-varying resistance is 300 mV (Fig. 12(a)), the signal frequency is 3.2 kHz and the filtering bandwidth

This manuscript was accepted by Rev. Sci.Instrum. Click here to see the version of record.

of 1 Hz. The measurement has been performed in three different conditions: i) using the commercial HF2LI by Zurich Instruments; ii) using ELIA instrument as a standard lock-in amplifier (i.e. only measuring the DUT signal with a single acquisition channel); iii) using ELIA with f_{SW} set to 1 kHz and performing the ratiometric technique. The resolution improvement of more than one order of magnitude, from 9 ppm to 0.6 ppm, given by the switched ratiometric technique, allows a clear detection of the tiny (5 ppm) resistance modulation, which is completely masked by noise in standard LIA implementations, as reported in Fig. 12(b).

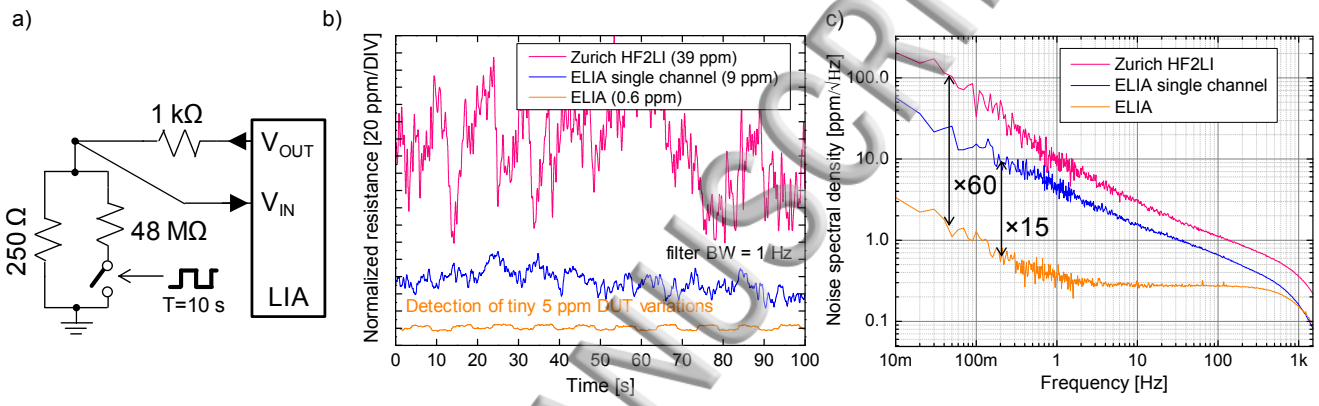

FIG. 12. Comparison of performance between standard LIA implementations and the switched ratiometric ELIA instrument. Thanks to the better performance of the latter, 5 ppm DUT variations produced by the experimental setup in (a) are measurable (b). The improvement is also apparent in the frequency domain as shown in (c). The spectra are obtained by setting the bandwidth of the LIAs at 650 Hz and by using a switching frequency of f_{SW} = 2 kHz.

Fig. 12(c) shows the measured noise spectra at the LIAs output in the same three experimental conditions. To obtain noise spectra going up to about one kHz, the LIAs frequency has been increased at 100 kHz, the filtering BW at 650 Hz, the switches frequency has been selected to f_{SW} = 2 kHz and the modulation of the DUT resistance has been disabled. The spectra clarify that the performance improvement given by the switched ratiometric technique is due to a substantial reduction of the 1/f noise affecting standard implementations. Moreover, the noise spectra show that the technique reduces the noise in the full measured bandwidth 0-1 kHz.

C. Independence from the Amplitude and Phase of DUT and STIM Signals

Differently from a differential technique that requires a precise matching between the signal path and the reference path, the effectiveness of the switched ratiometric technique is in principle insensitive to the phase and amplitude relationship between the DUT and STIM signals. In order to experimentally prove it, the instrument has been tested with an R-RC network. Fig. 13(a) shows the measured transfer function

of the tested network, characterized by a change of a factor 5 of the amplitude and of 45° of the phase with respect to the STIM signal. In Fig. 13(b) is shown the measurement resolution at every specific frequency. Sub-ppm performance (<1 ppm) has been achieved up to about 5 MHz, demonstrating an operation insensitive to the signal phase and amplitude.

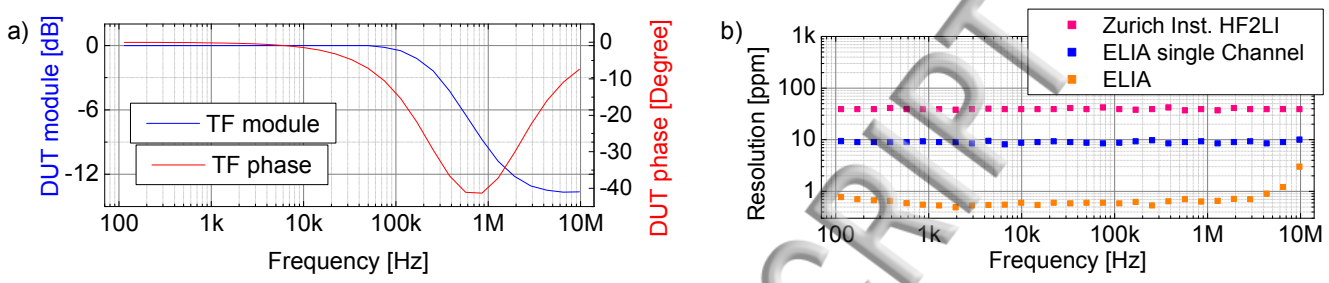

FIG. 13. Measured transfer function (a) of a complex impedance network used to assess the effect of amplitude and phase changes of the DUT signal. The resolution is below 1 ppm up to about 5 MHz independently of the DUT signal changes with respect to the STIM one (b).

The performance degradation observed for frequencies higher than 5 MHz can be explained by the channel transfer function (Fig. 14). At 6 MHz, it is decreased by 2% due to anti-aliasing filtering and is starting to rapidly decrease. The capacitors used in the anti-aliasing filters become increasingly important in defining the transfer function. They are characterized by a poor thermal coefficient of 30 ppm/K, thus possibly decreasing the resolution performance (about 3 ppm at 10 MHz) due to gain fluctuations induced by temperature variations.

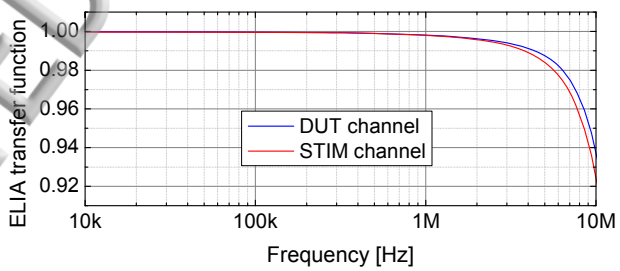

FIG. 14. Detail of the measured transfer functions of both DUT and STIM channels.

The insensitivity of the ELIA instrument to the amplitude and phase of the DUT signal with respect to the STIM signal, allows it to operate as a standard LIA, which does not require calibration steps at any new experiment or measurement frequency change, as happen with a differential approach.

D. Resolution and Switching Frequency

This manuscript was accepted by Rev. Sci.Instrum. Click here to see the version of record.

Consistently with the discussion in the section III-C, a relation between the switches frequency f_{SW} and the instrument resolution has been experimentally observed. Figure 15(a) shows the noise spectrum obtained with the ELIA instrument operated using a single channel (the DUT channel) as in standard LIA implementations. The stimulus frequency has been set to 500 kHz and the instrument output directly connected to the input. The obtained 1/f noise corner frequency f_c is about 1 kHz. Figure 15(b) shows the resolution obtained enabling the switched ratiometric technique and varying f_{SW}. The filtering bandwidth was 1 Hz and each measurement was 100 s long. With a switching frequency greater than 1 kHz the resolution flats on sub-ppm values. On the contrary, by lowering f_{SW} the resolution gets worse due to the overlapping with the side harmonics 1/f noise as discussed in section III-C. The time domain interpretation is that a significant gain fluctuation occurs during the switching period, thus the ADC gain experienced by the DUT and STIM signals is different.

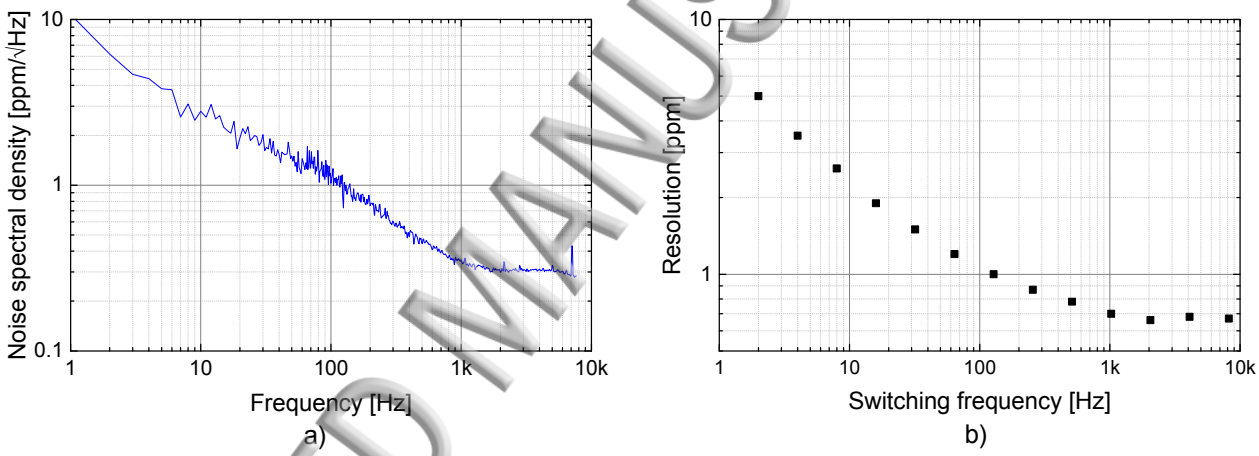

FIG. 15. a) Measured noise at the output of the instrument without the switching ratiometric technique. A noise corner of $f_c \approx$ 1 kHz is measured. B) Resolution dependence on the switching frequency in the case of BW = 1 Hz. To achieve the best performance the condition $f_{SW} > f_c + BW$ (Eq. 15) needs to be satisfied.

The effect of the switching frequency has been further investigated by making a sweep of the switching frequency f_{SW} from 320 Hz to 1.1 kHz at a fixed lock-in frequency of $f_0 = 990$ Hz and a filtering bandwidth BW = 1 Hz. Figure 16 shows the resolution measured as a function of the switching frequency. As predicted in III-C, in this frequency range, the measurement resolution gets worse for $f_{SW} \approx f_0$, $f_{SW} \approx 2/3 f_0$ and $f_{SW} \approx 2/5 f_0$. The greater worsening happens at $f_{SW} = f_0$ due to the feedthrough signal given by the switches commutations at the signal frequency f_0. The best resolution is obtained by shifting the switching frequency away from the cases $f_{SW} = 2f_0/(1+2k)$ of only ≈ 20 Hz. A slower recovery has been observed around $f_{SW} = f_0$, requiring a frequency shift of about 100 Hz. The results demonstrate that a suitable switching frequency is easily found also around these critical signal frequencies.

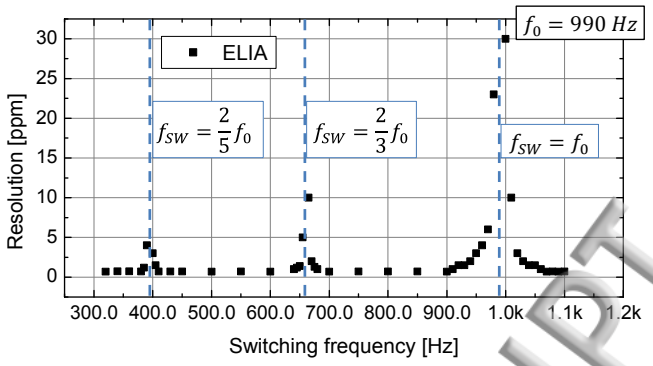

FIG. 16. Measured resolution as a function of the switching frequency. The LIA frequency is constant at f_0 = 990 Hz.

V. CONCLUSIONS

The best measurement resolution achievable using lock-in amplifiers is limited by an underestimated 1/f noise in the demodulated signal proportional to the signal to be measured. The measurement resolution is limited by such noise and cannot be improved narrowing the filtering bandwidth, because the noise is 1/f, neither increasing the signal amplitude, because the noise is proportional to the signal, thus posing a fundamental limit.

The source of the 1/f noise limiting the resolution has been identified in the effect of gain fluctuations of various elements of the generation and acquisition chain. In particular, the gain fluctuations are added by the digital-to-analog and analog-to-digital converters.

A differential approach reduces the effects of the gain fluctuations, enabling the measurement of small variations. However, it requires the design of a reference path matched to the signal path for all the experimental conditions. In order to simplify the experimental setup and avoid a calibration step of the reference, a LIA based on two ADCs alternately acquiring the signal coming from the Device Under Test (DUT) and the stimulus (STIM) signal, has been conceived and implemented. This enhanced-LIA allows the compensation of the slow gain fluctuations of both DAC and ADC, considerably reducing their effect on the measurements. Experimental results demonstrate the effectiveness of the technique, improving the instrumentation resolution limit by a factor 15, from 9 to 0.6 ppm. Such a resolution value is considerably better than the examined state-of-the-art LIA standard implementations working up to similar frequencies, as shown in Table 1.

The technique does not require additional external elements or accurate case-by-case calibrations, two typical constraints of the alternative differential technique. Instead, it only requires choosing the switching

frequency few hundred of Hz away from the signal frequency, a condition easily implemented in the firmware of the instrument.

ACKNOWLEDGMENTS

The authors would like to thank F. Campoli for his experimental work. They are also grateful to M. Sampietro for the valuable contributions towards this research effort. This work was supported by Fondazione Cariplo under project DRINKABLE (grant no. 2014-1285) and by the European Union through project H2020-ICT- STREAMS (grant no. 688172).

REFERENCES

1 M.L. Meade, "Lock-in Amplifiers: Principles and Applications" London: Peter Peregrinus Ltd., 1983.

2 S. Chen, H. C. Hsiung, W. Su, D. P. Tsai, "Convenient near-field optical measurement and analysis of polystyrene spheres", Vacuum, vol. 81, pp 129-132, 2006.

3 Y. Li, N. Zhou, A. Raman, X. Xu, "Three-dimensional mapping of optical near field with scattering SNOM", Optics Express, vol. 23, issue 14, pp 18730-18735, 2015.

4 C. W. Freudiger, W. Min, B.G. Saar, G. R. Holtom, C. He, J. C. Tsai, J. X. Kang, X. S. Xie, "Label-Free Biomedical Imaging with High Sensitivity by Stimulated Raman Scattering Microscopy", Science, Vol. 322, Issue 5909, pp. 1857-1861, Dec. 2008

5 J. Wei, C. Yue, M. van der Velden, Z. L. Chen, Z. W. Liu, K. A. A. Makinwa, and P. M. Sarro, "Design, fabrication and characterization of a femto-farad capacitive sensor for pico-liter liquid monitoring", Sensors Actuators A Phys., vol. 162, no. 2, pp. 406–417, 2010.

6 N. Haandbæk, O. With, S. C. Bürgel, F. Heer, and A. Hierlemann, "Resonance-enhanced microfluidic impedance cytometer for detection of single bacteria.," Lab Chip, pp. 3313–3324, 2014.

7 C. Azzolini, A. Magnanini, M. Tonelli, G. Chiorboli, and C. Morandi, "A CMOS vector lock-in amplifier for sensor applications," Microelectronics J., vol. 41, no. 8, pp. 449–457, 2010.

8 J. Woo, J. Cho, C. Boyd, K. Najafi, "Whole-angle-mode micromachined fused-silica birdbath resonator gyroscope (WA-BRG)", Micro Electro Mechanical Systems (MEMS), 2014 IEEE 27th International Conference on, 2014

9 G. Gervasoni, M. Carminati, G. Ferrari, M. Sampietro, E. Albisetti, D. Petti, P. Sharma, and R. Bertacco, "A 12-channel dual-lock-in platform for magneto-resistive DNA detection with ppm resolution," in *2014 IEEE Biomedical Circuits and Systems Conference (BioCAS) Proceedings*, pp. 316–319, 2014.

10 M. Carminati, A. Rottigni, D. Alagna, G. Ferrari, M. Sampietro, "Compact FPGA-based elaboration platform for wide-bandwidth electrochemical measurements", in 2012 IEEE I2MTC—International Instrumentation and Measurement Technology Conference, Proceedings, no. 214706, pp. 264–267, 2012

11 M. Carminati, G. Gervasoni, M. Sampietro, and G. Ferrari, "Note: Differential configurations for the mitigation of slow fluctuations limiting the resolution of digital lock-in amplifiers," Rev. Sci. Instrum., vol. 87, no. 2, p. 026102, Feb. 2016.

12 M. C. Foote and A. C. Anderson, "Capacitance bridge for low temperature, high-resolution dielectric measurements," Review of Scientific Instruments, vol. 58, no. 1, p. 130, 1987.

13 AH 2700A, Andeen-Hagerling.

14 M. A. P. Pertijs, K. A. A. Makinwa, and J. H. Huijsing, "A CMOS smart temperature sensor with a 3σ inaccuracy of ±0.1°C from -55°C to 125°C," IEEE J. Solid-State Circuits, vol. 40, no. 12, pp. 2805–2815, Dec. 2005.

15 K. Mochizuki, T. Masuda, and K. Watanabe, "An interface circuit for high-accuracy signal processing of differential-capacitance transducers," IEEE Trans. Instrum. Meas., vol. 47, no. 4, pp. 823–827, 1998.

16 S. Pennisi, "High-Performance and Simple CMOS Interface Circuit for Differential Capacitive Sensors," IEEE Trans. Circuits Syst. II Express Briefs, vol. 52, no. 6, pp. 327–330, 2005.

17 PerkinElmer, Low Level Optical Detection using Lock-in Amplifier Techniques, 2000.

18 G. Ferrari, G. Gervasoni, M. Carminati, F. Campoli, patent application PCT/IB2017/050877 of 16.02.2017.

19 G. Gervasoni, M. Carminati, G. Ferrari, "FPGA-based lock-in amplifier with sub-ppm resolution working up to 6 MHz", Electronics, Circuits and Systems (ICECS), 2016 IEEE International Conference on, 2016.

This manuscript was accepted by Rev. Sci.Instrum. Click here to see the version of record.

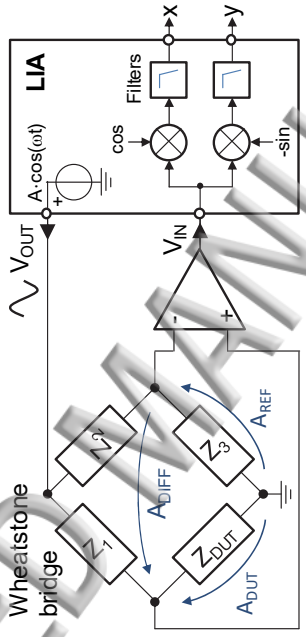

This manuscript was accepted by Rev. Sci.Instrum. Click here to see the version of record.

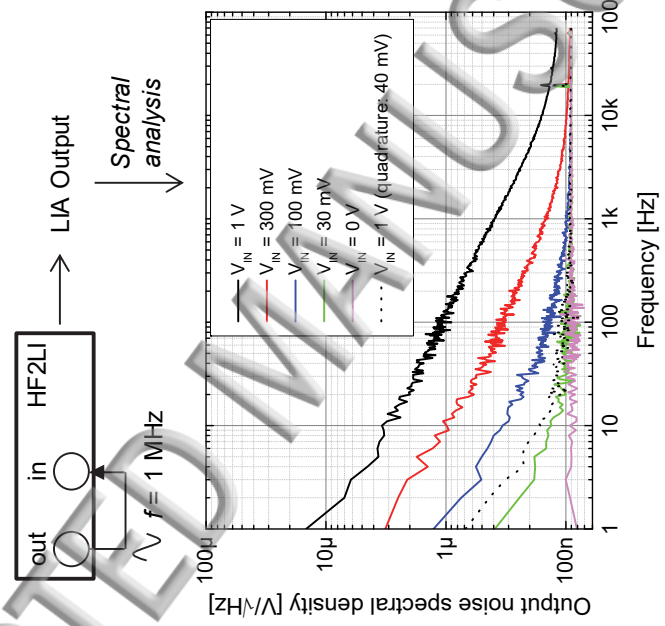

This manuscript was accepted by Rev. Sci.Instrum. Click here to see the version of record.

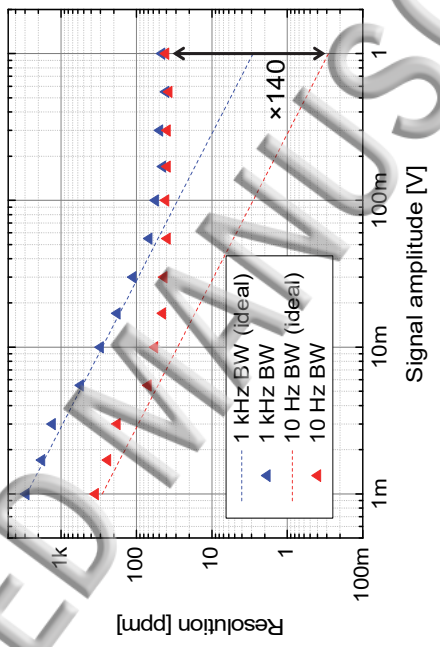

This manuscript was accepted by Rev. Sci.Instrum. Click here to see the version of record.

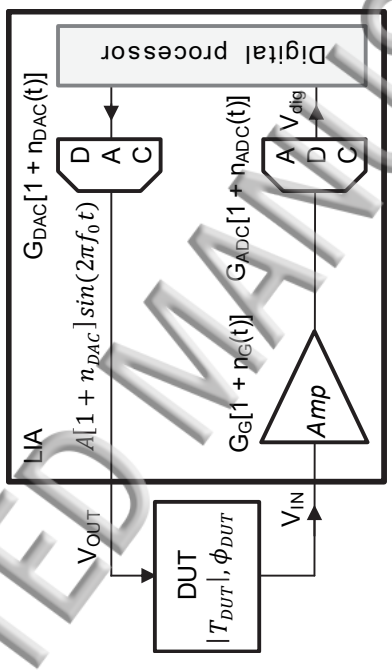

This manuscript was accepted by Rev. Sci.Instrum. Click here to see the version of record.

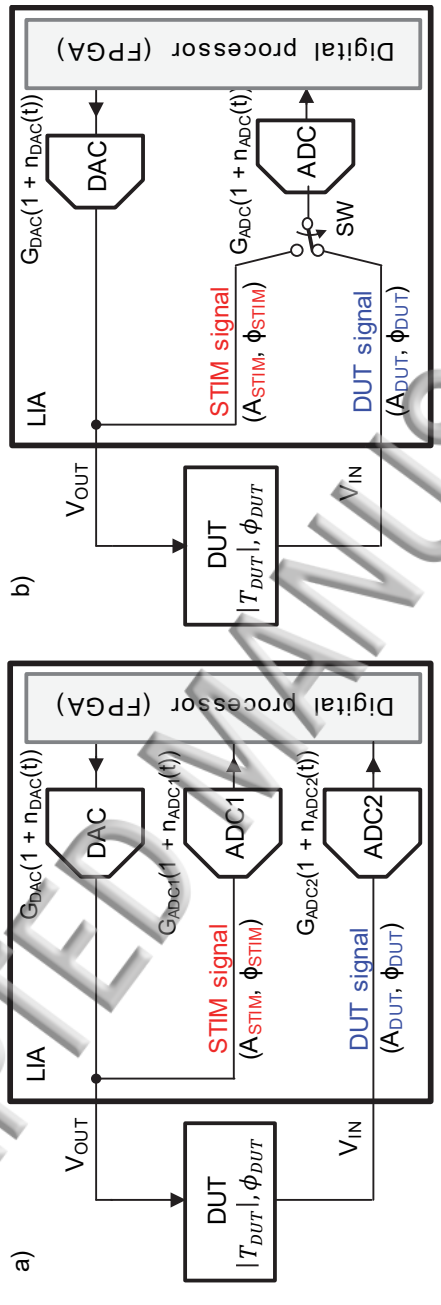

$$A_{DUT} = A|T_{DUT}| \cdot (1 + n_{DAC}(t)) \cdot (1 + n_{ADC1}(t))$$
$$A_{STIM} = A \cdot (1 + n_{DAC}(t)) \cdot (1 + n_{ADC2}(t))$$
$$A_{DUT}/A_{STIM} = |T_{DUT}| \cdot (1 + n_{ADC1}(t))/(1 + n_{ADC2}(t))$$

$$A_{DUT} = A|T_{DUT}| \cdot (1 + n_{DAC}(t)) \cdot (1 + n_{ADC}(t))$$
$$A_{STIM} = A \cdot (1 + n_{DAC}(t)) \cdot (1 + n_{ADC}(t))$$
$$A_{DUT}/A_{STIM} = |T_{DUT}|$$

This manuscript was accepted by Rev. Sci.Instrum. Click here to see the version of record.

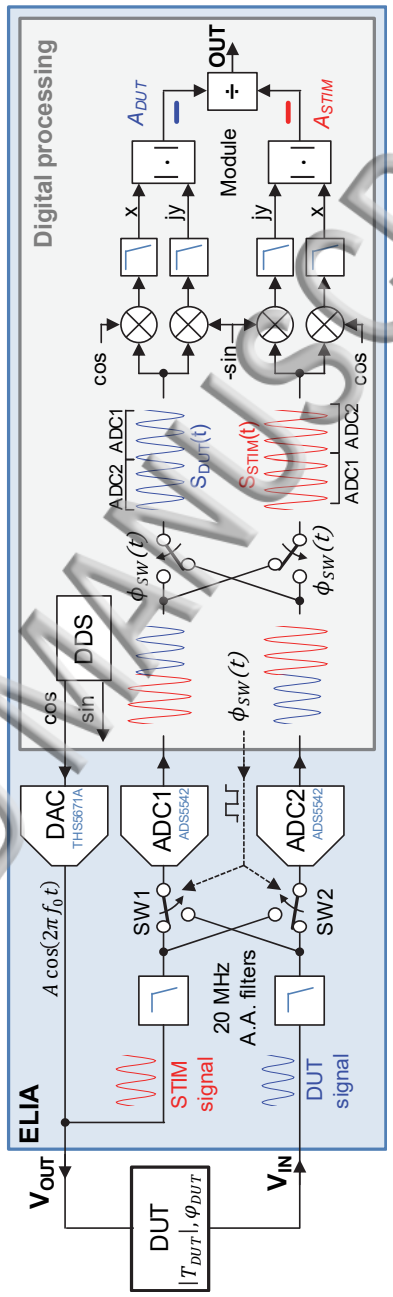

This manuscript was accepted by Rev. Sci.Instrum. Click here to see the version of record.

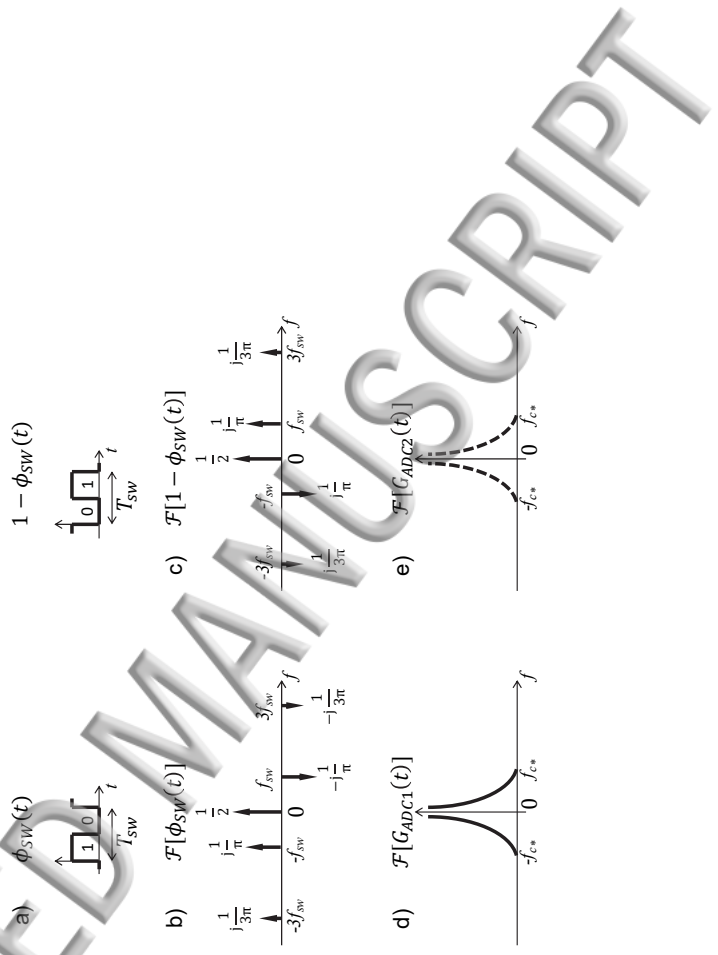

This manuscript was accepted by Rev. Sci.Instrum. Click here to see the version of record.

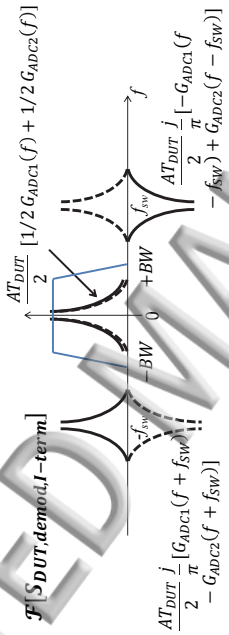

This manuscript was accepted by Rev. Sci.Instrum. Click here to see the version of record.

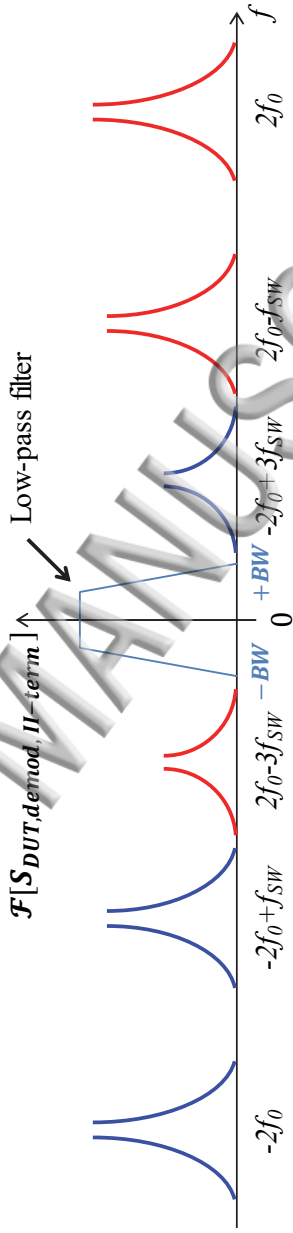

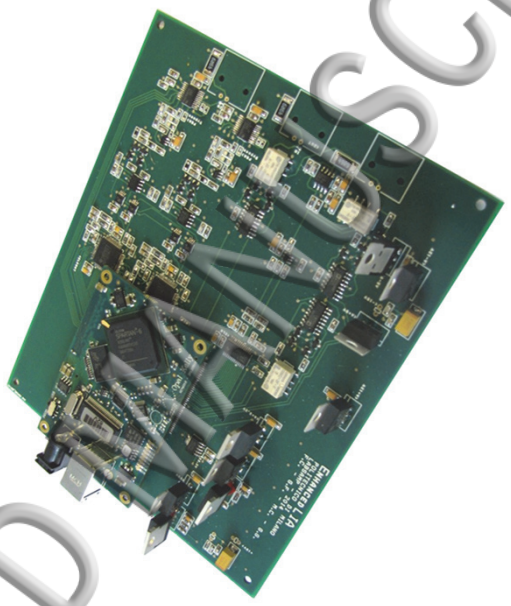

This manuscript was accepted by Rev. Sci.Instrum. Click here to see the version of record.

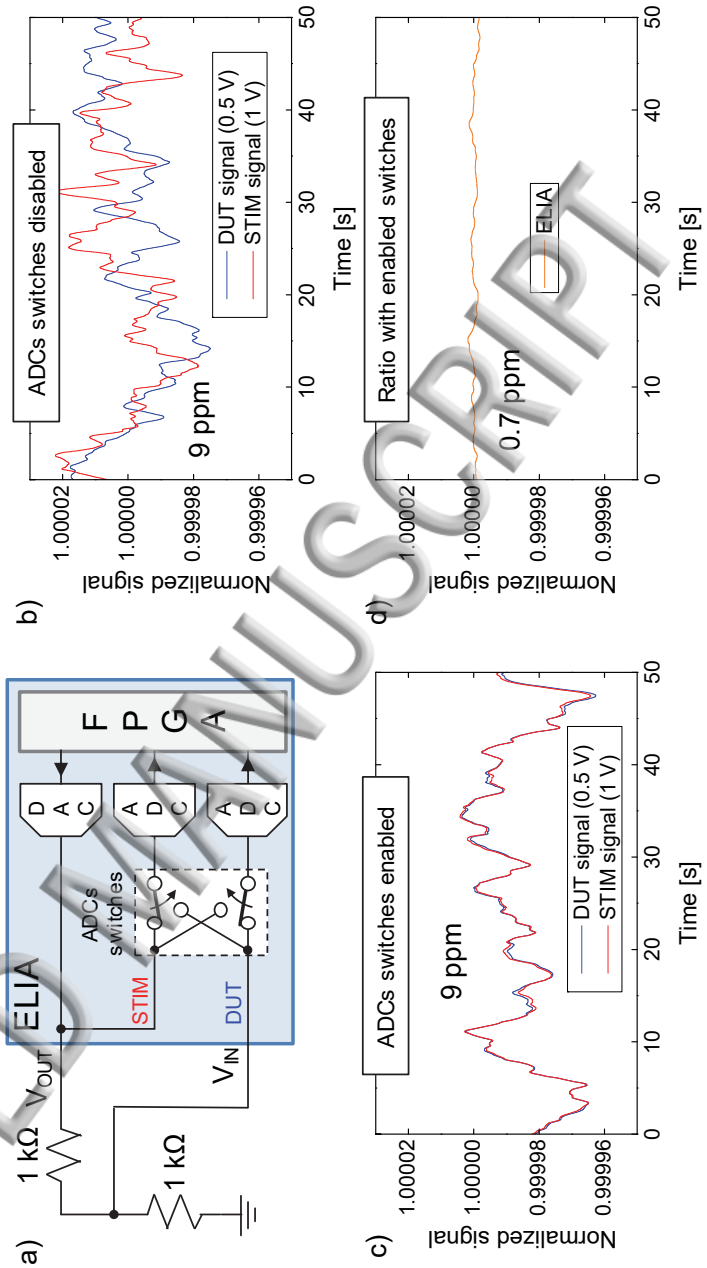

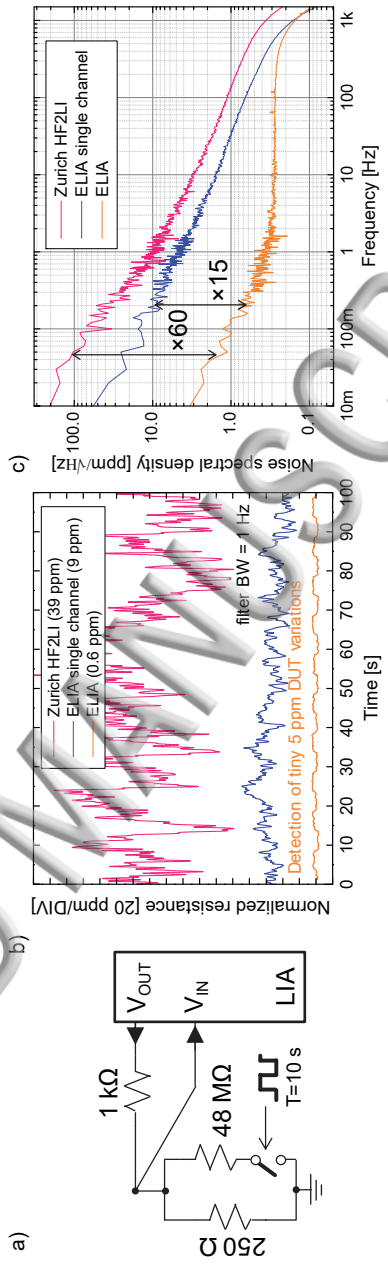

This manuscript was accepted by Rev. Sci.Instrum. Click here to see the version of record.

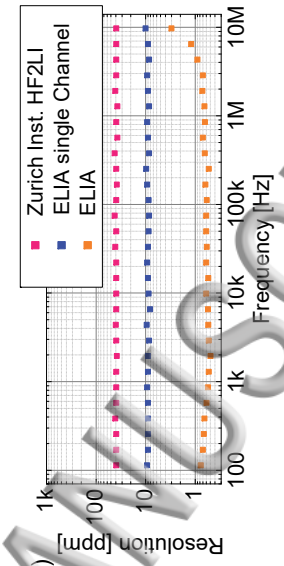

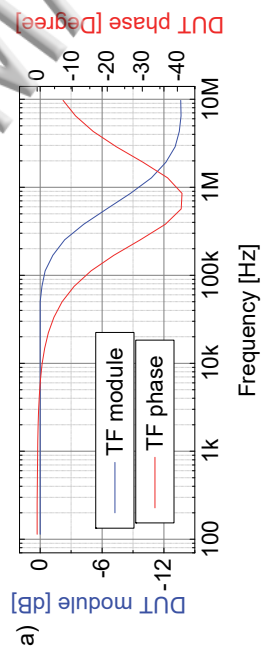

This manuscript was accepted by Rev. Sci.Instrum. Click here to see the version of record.

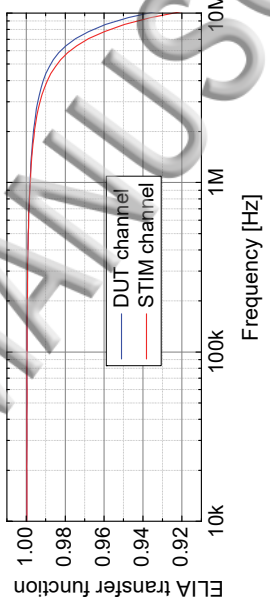

This manuscript was accepted by Rev. Sci.Instrum. Click here to see the version of record.

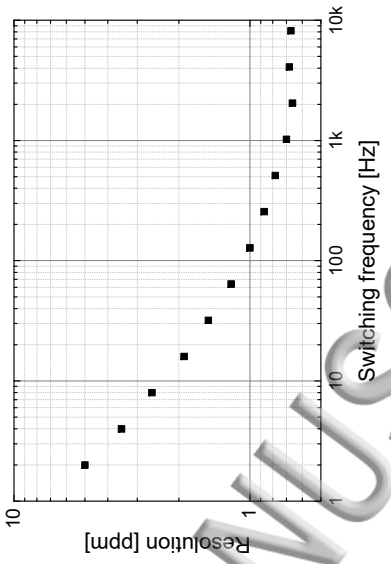

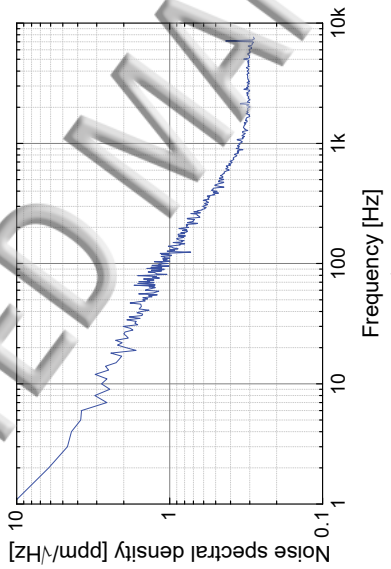

This manuscript was accepted by Rev. Sci.Instrum. Click here to see the version of record.